



Juice/SWI during the Lunar-Earth-Gravity-Assist.

III. Observations of the Earth as Calibration Target

Christopher Jarchow¹, Ladislav Rezac¹, Paul Hartogh¹, Ali Schulz-Ravanbakhsh¹, Thibault Cavalié², Fabrice Herpin², Raphael Moreno³, and Axel Murk⁴

¹Max-Planck-Institut für Sonnensystemforschung, Justus-von-Liebig-Weg 3, 37077 Göttingen, Germany

²Univ. Bordeaux, CNRS, LAB, UMR 5804, F-33600 Pessac, France

³LIRA - Laboratoire d'Instrumentation et de Recherche en Astrophysique, Observatoire de Paris, Section de Meudon, 5, place Jule Janssen - 92195 MEUDON Cedex

⁴Univ. Bern, Institute of Applied Physics, Sidlerstrasse 5, 3012 Bern, Switzerland

Correspondence: Christopher Jarchow (jarchow@mps.mpg.de)

Abstract. On August 19th and 20th 2024 the *Jupiter Icy Moons Explorer* (Juice) executed during its cruise phase towards Jupiter a combined *Lunar Earth Gravity Assist* (LEGA) maneuver. These close flybys of the Moon and the Earth provided so far the best opportunity to test the behavior, performance, and calibration of the *Submillimetre Wave Instrument* (SWI) onboard Juice. This paper shows typical data taken during the Earth Gravity Assist and the following few days. Data quality and problems resulting from unexpected behavior of the hardware are discussed.

1 Introduction

The *Submillimetre Wave Instrument* (SWI) onboard Juice is essentially a 29-cm single dish radio telescope operating simultaneously in the two frequency bands 530–638 GHz and 1066–1286 GHz. Though the instrument's nominal functional and performance tests have been carried out already during the *Near Earth Commissioning Phase* (NECP) from May to July 2023, the combined *Lunar Earth Gravity Assist* (LEGA) provides a unique test environment to investigate in much more detail the performance and behavior of SWI in space. For the first time after the launch of Juice on 14 April 2023 the following kind of tests could be performed:

- The close distance of only about 6800 km to the Earth's surface during closest approach of the *Earth Gravity Assist* allowed to perform true limb sounding of the Earth's atmosphere. This observation geometry provides the largest spectral line contrast in brightness temperature during the entire cruise phase of Juice. It was necessary to check, if the instrument can measure and process such an input signal in the expected way.
- In addition this small distance between the Earth and the spacecraft allowed to observe the Earth as a target which fills the complete antenna pattern of the instrument – even a few days after closest approach the Earth had an apparent diameter of still ten to thirty times the full beam width of the instrument. This condition allows to check the total power calibration approach without detailed knowledge of the various telescope efficiency numbers (see e.g. Kutner and Ulich, 1981), first of all the telescope main beam efficiency.



- The high brightness temperature level of the Earth’s continuum radiation allowed a fast detection and evaluation of possible standing wave patterns created in the optical path of SWI’s telescope.
- In general, the close distance and large apparent size of the Earth provided such a strong input signal to the instrument that spectral lines of water vapor, ozone, and oxygen could be detected within only a few seconds of integration time. This was not possible during NECP, because during that time the Earth’s apparent diameter was only a fraction of SWI’s beam width and the received signal was simply too weak. As a consequence the LEGA provided for the first time the opportunity to test the instrument’s performance over the entire spectral tuning range.
- The huge amount of various optically thick and thin spectral transitions in the Earth’s atmospheric spectrum, in combination with observations requiring only short integration times, provide a comprehensive data set to test and study the instrument’s end-to-end measurement performance.
- The high spectral density and large number of closely spaced ozone spectral lines originating in the Earth’s atmosphere allowed us to investigate and evaluate the behavior of the side band ratio for different tunings of the instrument.
- Finally scans across the sharp edge of the Earth’s disk towards cold space provide data which allow an estimate of SWI’s antenna pattern (Moreno et al., 2026, this issue). Especially the beam width of the pattern’s main lobe could be measured with sufficient quality to verify the optical design of the telescope.

The basic idea of the analysis of SWI’s LEGA data is to consider the Earth as a well-known target and to compare the observation results with theoretically *expected results*. Any deviation of the observations from the expectations is then considered primarily as an *instrumental effect*. However, this approach should not be taken as a strict rule: it is always possible that the Earth shows an unexpected behavior, which simply has not been taken into account in the modeling of the expected spectra. For example, currently we do not take into account small scale local atmospheric variations of clouds and tropospheric water vapor, which may be well resolved by the instrument at the extreme close distance to the Earth around the closest approach.

This paper presents typical data obtained during LEGA and provides an overview of the current status of the ongoing data analysis to better understand the instrument behavior and related systematic measurement errors.

2 Instrument Description

There are a few things about SWI the reader needs to know to better understand the data presented in this paper: SWI is essentially a small 29-cm single dish radio telescope. Using a polarizing grid as beam splitter behind the primary, secondary and tertiary mirrors of the telescope optics, the received electromagnetic radiation is fed into two independent heterodyne receivers, which are usually operated simultaneously. The two receivers are both tunable and operate in the frequency range of 530–638 GHz respectively 1066–1286 GHz. Each of the two receivers is equipped with two different spectrometers: a *chirp transform spectrometer* (CTS) and a digital *autocorrelation spectrometer* (ACS). The CTS analyses the intermediate frequency



signal in the range of 5.5–6.5 GHz with 10000 equidistant channels (i.e. 1 GHz instantaneous bandwidth with 100 kHz resolution), while the ACS analyzes the intermediate frequency signal in the range of 4.4–8.8 GHz with 1024 equidistant channels (i.e. 4.4 GHz instantaneous bandwidth with 4.3 MHz resolution). At any time only one type of these two different spectrometers
55 can be operated: either both receivers use the CTS or the ACS. Examples of spectra taken with these two kind of spectrometers are shown in section 4.3.

It is important to keep in mind that the receivers of SWI are so-called *double sideband* receivers, which are sensitive for two frequency bands at the same time: the *upper sideband* (USB) at frequencies given by the local oscillator frequency plus the intermediate frequency and the *lower sideband* (LSB) frequencies given by the local oscillator frequency minus the intermediate
60 frequency. As a consequence two spectral line transitions with sky frequencies differing by e.g. 12 GHz will show up at the same intermediate frequency in the CTS spectrum. It is not possible to separate the two contributions from the two sidebands and then to show them separately as function of the sky frequency. Instead it is easier to always show the data as function of the intermediate frequency (IF) and to set up the theoretical models in a way to also provide double sideband data.

For more information see also Hartogh et al. (2026b, this issue); a detailed description of the instrument can also be found
65 in Hartogh et al. (2026a, in preparation).

2.1 Total Power Calibration Approach

The challenge in spectro radiometric observations is the precise calibration of the received radiation intensity into physical units. A well-designed and properly built instrument always shows a linear relationship between the received radiation intensity (specified as Rayleigh-Jeans brightness temperature) and the observed IF-power.

70 To calibrate the received radiation intensity emitted by a science target – here the Earth – it is always necessary to observe two reference blackbody loads of known, different physical temperature – the *hot load* at temperature T_h and the *cold load* at temperature T_c . Observing these two loads provide two points (T_c, P_c) and (T_h, P_h) , which allow to determine the two coefficients a and b of the linear calibration curve $P(T) = ax + b$ (see Figure 1). Knowing the calibration curve then allows to calibrate any received power P_a in terms of the corresponding brightness temperature T_a :

$$75 \quad T_a = \frac{T_h(P_a - P_c) - T_c(P_a - P_h)}{P_h - P_c} \quad (1)$$

It is also possible to calculate the receiver noise temperature T_n , which corresponds to the observed power for a target at a temperature of zero Kelvin (i.e. which does not emit at all):

$$T_n = \frac{T_h P_c - T_c P_h}{P_h - P_c} \quad (2)$$

SWI uses the cold sky as calibration cold load, which has a brightness temperature of essentially zero Kelvin at the observed
80 frequencies. Entering $T_c = 0$ into equation 1 and 2 simplifies these equations to

$$T_a = \frac{T_h(P_a - P_c)}{P_h - P_c} \quad (3)$$

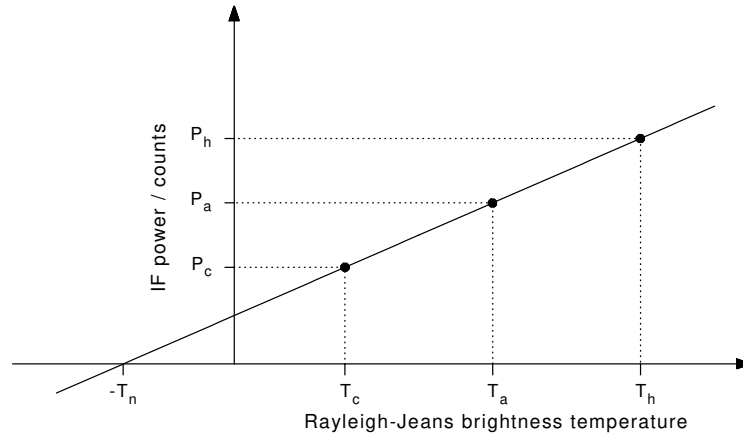


Figure 1. Illustrates the standard two-load total power calibration scheme using a *hot* and a *cold* load at different temperatures.

and

$$T_n = \frac{T_h P_c}{P_h - P_c} \tag{4}$$

If the instrument would be perfectly stable it would be sufficient to determine the calibration curve only once and then to
 85 calibrate any observed power P_a to the corresponding brightness temperature T_a . However, in practice the instrument is not
 stable: both the slope of the calibration curve and the noise temperature T_n do vary with time and environmental conditions.
 Especially temperature variations (e.g. caused by the instrument warm-up after power-on) cause a change of the amplification
 gain of various amplifiers within both the receiver and the spectrometer hardware, which translates directly into a change of
 the slope of the calibration curve. In addition temperature changes of the mixer diodes within the receiver hardware causes
 90 changes of the receiver noise temperature itself.

To compensate for such a variation it is necessary to periodically repeat the observations of the hot and cold load in order to
 obtain the correct calibration curve close to the time of any observation. The time interval between these periodic observations
 of the calibration loads depends solely on the stability and drift behavior of the instrument. It just has to be determined by
 observing the instrumental drift behavior under operational conditions (see e.g. Schieder and Kramer (2001) and Ossenkopf
 95 (2008) for a detailed discussion of this issue). As a rule of thumb usually this time interval between the periodic observations
 of the calibration loads is on the order of 10 to 30 seconds.

2.2 The Calibration Flip Mirror Issue

To properly perform the described calibration procedure SWI is equipped with an *internal hot load* and a so-called *calibration*
flip mirror, which flips the receivers input signal from the telescope optics to the internal hot load (Hartogh et al., 2026b, this
 100 issue). Unfortunately, after launch it has been discovered that the flip mirror mechanism has a significantly reduced lifetime:
 instead of the required minimum of 54000 flip cycles the life time is currently estimated to about only 10000 cycles before the



mechanism finally gets mechanically stuck. This issue creates a serious problem for the intended usage of SWI. Therefore, the SWI team needs to find ways to reduce the amount of needed flip mirror cycles, and to find ways to perform the total power calibration without observing the internal hot load.

105 A possible way out of this situation has been provided by the empirical observation that the receiver noise temperature T_n is quite stable: repeating four times a measurement of T_n for a fixed set of 150 different tunings (75 tunings per receiver) shows a noise temperature depending on tuning, but for each tuning the individual measurements scatter only by about 4% around the median value. This behavior of the instrument suggests to replace the hot load observation by the nearly stable receiver noise temperature. Combining equation 3 and 4 allows to eliminate T_h and P_h :

$$110 \quad T_a = T_h \frac{P_a - P_c}{P_h - P_c} \quad (5)$$

$$= T_h \frac{P_c}{P_h - P_c} \frac{P_a - P_c}{P_c} \quad (6)$$

$$= T_n \frac{P_a - P_c}{P_c} \quad (7)$$

The expression $(P_a - P_c)/P_c$ allows to cancel out time variations of the slope of the calibration curve, as long as the time interval between the measurement of P_a and P_c is short enough. Performing Allan variance measurements under operational conditions helps to find the maximum length of this time interval (see e.g. Schieder and Kramer, 2001).

2.3 Observation Sequence

In practice this modified calibration approach means to execute any observation of a science target as a pair of observations: usually half of the total observing time is spent on the target while the other half is spent on cold sky. The SWI science observations are accomplished via different scripts or science modes that provide different ON/OFF calibration patterns (for a comprehensive summary see Cavalié et al., 2026, this issue). Depending on the stability of the instrument the total observing time needs to be split into many of such pairs with accordingly shortened observation time. In radio astronomy this approach is known as the so-called *position switched* observation sequence. An observation of the hot load is not done during the observation. Instead it is only necessary to have a trustworthy measurement of T_n , done at any time before or after the actual observation of the science target. Here the term *trustworthy* means to have a good idea how large the error of the used noise temperature is, i.e. how large the difference between the unknown noise temperature at the time of the science observation and the used noise temperature is. This knowledge can be only obtained by carefully and periodically monitoring the instrument behavior and its response to changing environmental temperatures – it is necessary to understand instrumental drift effects and take them properly into account.

3 Expected Spectra of the Earth

130 In order to evaluate the quality and measurement error of the SWI data it is necessary to have a model of the Earth capable to predict the expected data. The model consists of two parts: the first part is just the model of the Earth's atmosphere, i.e. the



altitude profiles of temperature, pressure, and the mixing ratios of water vapor, oxygen, and ozone, to cover the main spectral features, and the second part is the radiative transfer model, which calculates the brightness temperature spectrum of the Earth as seen by SWI from space for the given atmospheric profiles.

135 3.1 Earth Atmosphere Model

The atmospheric temperature, pressure, water vapor and ozone mixing ratio profiles used in this work have been taken from the *Modern-Era Retrospective Analysis for Research and Applications, Version 2 (MERRA-2)* database (Gelaro et al., 2017; Global Modeling And Assimilation Office and Pawson, 2015). This database provides these data with a time resolution of three hours and a spatial resolution of 0.5 degrees in latitude and 0.625 degrees in longitude. The data have been resampled the following
140 way: average over 24 hours in time, average over all longitudes (i.e. zonal average), and average over a 10 degree range in latitude (starting from the equator to 10 degrees, 10 to 20 degrees, 20 to 30 degrees, ...)

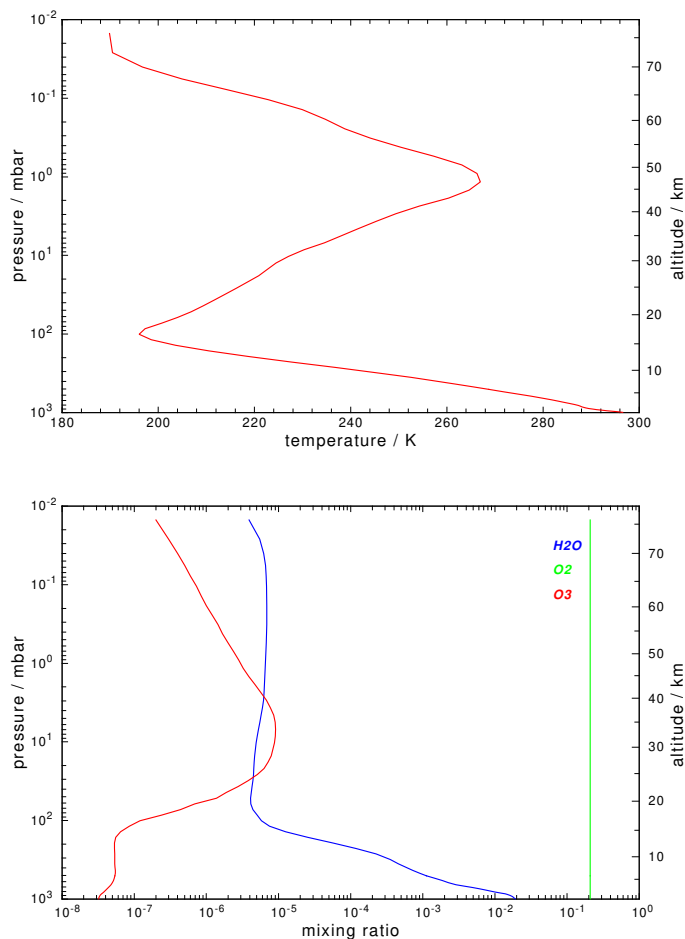


Figure 2. The temperature and mixing ratio profiles used in this work for the modeling of Earth spectra.



In this work we focus on the data analysis of SWI observations in nadir looking geometry. Because the sub-spacecraft latitude during the days after closest Earth approach has been varying between 16 and 17 degrees southern latitude, the Earth atmosphere model has been taken from the MERRA-2 data averaged between 10 and 20 degrees southern latitude. Within the days when the LEGA Earth observations were performed, these averaged profiles do not show significant time variations with date, so the data for the 22 August 2023 (see Figure 2) have been taken to represent the atmosphere for all Earth observations during the LEGA segment (20-23 August 2023).

3.2 Radiative Transfer Model

The radiative transfer model is a straight forward line-by-line and layer-by-layer model, which has been initially developed at MPS (Jarchow and Hartogh, 1995, 1997) and improved ever since. The atmosphere is represented by a stack of discrete layers of typically $\Delta x_i = 1$ km thickness, where the temperature, pressure, and mixing ratios in each layer is uniform (see Figure 3). The radiation $I(x_N)$ passing through such a stack of N layers can be calculated as

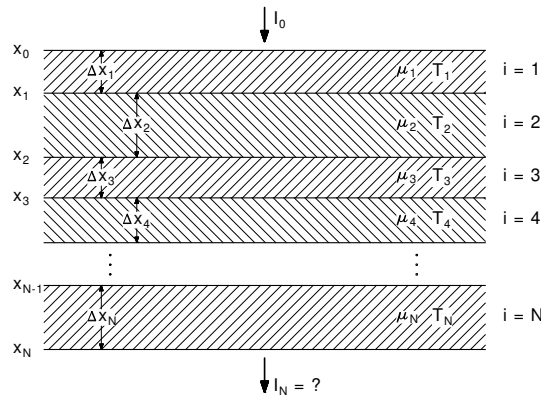


Figure 3. Illustration of the layer-by-layer approach used to calculate the radiation transfer through the Earth’s atmosphere.

$$I_N \equiv I(x_N) = I(x_0) e^{-\sum_{i=1}^N \mu_i \Delta x_i} + \sum_{i=1}^N J_i \mu_i e^{-\sum_{j>i}^N \mu_j \Delta x_j} \Delta x_i \quad (8)$$

In case of a medium in thermodynamic equilibrium the source function J_i is given for each layer i by the Planck function

$$J_i(\nu, T) = \frac{2h\nu^3}{c^2} \frac{1}{e^{h\nu/hT} - 1} \quad (9)$$

where T denotes the temperature and ν the frequency. Each layer’s absorption coefficient μ_i is given by

$$\mu_i(\nu, T) = N \cdot \frac{\nu}{\nu_0} \cdot f(\nu, \nu_0) \cdot I_{ab}(T) \quad (10)$$

where N is the number density of the emitting resp. absorbing molecules, ν_0 the transition frequency of the spectral line under consideration, and $f(\nu, \nu_0)$ the spectral line shape function, which takes into account the pressure broadening effect caused by



160 molecular collisions and the Doppler broadening effects caused by the thermal movement of the molecules. Here our radiative
transfer code uses always the Voigt function, which is the convolution of a Lorentz function with a Gauss function. The Zeeman
splitting of the oxygen transitions has not been taken into account in our radiative transfer model. As a consequence the model
is currently not suitable to derive mesospheric temperatures from the oxygen transitions at 1120.7 and 1179.9 GHz, which both
have been observed by SWI during LEGA. Finally the spectral line intensity $I_{ab}(T)$ has been calculated using the HITRAN
165 2008 spectral line catalog (Rothman et al., 2009).

In case of several different molecular species and several spectral line transitions for each of these species the absorption
coefficient needs to be calculated for each transition and each species separately and then these individual contributions finally
need to be summed up to obtain the total absorption. Hence our model belongs to the line-by-line radiation transfer models.

4 Results

170 4.1 Total Power Calibration

The LEGA observations of the Earth offer the first opportunity to evaluate the SWI calibration approach as described in
sections 2.1 and 2.2. The idea here is to focus on those observations when the instrument was pointing towards Earth's center,
i.e. to analyze all observations with a nadir looking geometry. This approach has several advantages:

- Because of the close distance of the Earth during LEGA its apparent size is much larger than the beam width, so the Earth
175 is essentially filling the entire beam. Thus no detailed knowledge of the beam pattern is needed, instead the expected
spectra can be calculated using a simple pencil beam geometry for the radiative transfer.
- The data do not strongly depend on the exact pointing (contrary to e.g. limb viewing geometry). A miss-pointing on the
order of a couple of beam-widths would not cause a significant change of the observed signal.
- No limb darkening or brightening effects need to be taken into account, because SWI sees only a small fraction of the
180 apparent disk around its center.

Another important thing simplifying the calculation of the expected Earth spectrum is given by the fact that the strong water
vapor transitions within SWI's frequency range do not allow the ground emission to reach the instrument. For SWI the Earth
simply looks like a gas planet with water vapor in the altitude range of 6 to 16 km providing the continuum background radia-
tion. However, this situation does also provide some challenge: the continuum level depends critically on the exact temperature
185 and water vapor concentration within this altitude range.

All of the observations executed during LEGA have been searched for nadir viewing spectra. These data have been found
in 1- and 2-dimensional mapping observations (observation script name SWI_2D_MAP_OTF_V1) and spectral scans (ob-
servation script name SWI_SPECTRAL_SCAN_CTS_PS_V1 and SWI_SPECTRAL_SCAN_ACS_PS_V1). For a detailed
description of these observation modes see Cavalié et al. (2026, this issue). In this work only observations involving the CTS
190 are shown, the observations and analysis involving the ACS will be presented in a future publication.



4.1.1 1-Dimensional Maps

The observing scheme for 1- and 2-dimensional maps differs from the general principle described in section 2.3. Instead of a set of *target–sky* pairs the target is observed *on-the-fly*, i.e. the target is rastered pixel by pixel without an intended observation of cold sky in-between (Ossenkopf, 2009). Instead cold sky data are automatically observed by simply setting the size of the map larger than the size of the target. An example of a 1-dimensional map is show in Figure 4. It can be easily seen that

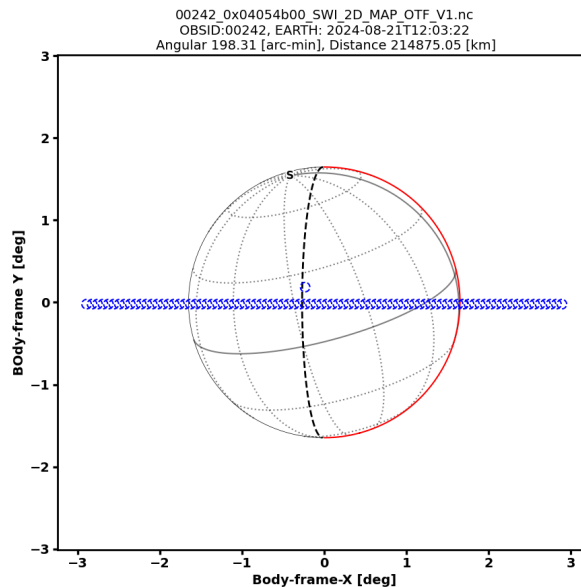


Figure 4. Example (ObsID 242) of the observing geometry for a 1-dimensional scan across the Earth’s disk in East–West direction. The blue circles represent the position and beam size of the low frequency or so-called *600 GHz* receiver. At the position of each circle an individual measurement or spectrum of 1.5 seconds integration time has been taken.

195

the cold sky has been observed twice, once at the begin and a second time at the end of the observation. Averaging these spectra to a single P_c reference spectrum then allows to calculate the quantity $(P_a - P_c)/P_c$ for all of the pixels of the 1-dimensional scan. Multiplying all of these 'partly' calibrated pixels with a single T_n spectrum obtained from a former or later measurement – which made use of the instrument internal hot load – then results in absolute scale calibrated data. Without explicitly mentioning a spectral channel index j in the equations it still needs to be understood that each pixel is associated with an entire CTS spectrum of 10000 channels. Averaging these 10000 channels to a single number for each individual pixel finally provides a simple overview of the observation versus time. Figure 5 shows such kind of overview for the two spectrometers CTS1 and CTS2, respectively for the two receivers (CTS1 is connected to the 600 GHz receiver and CTS2 is connected to the 1200 GHz receiver). It can be clearly seen that the brightness temperature for the cold sky observing parts are close to zero and on the same level before and after crossing the Earth’s disk. This indicates a stable instrument during the observation and justifies the on-the-fly approach a posteriori. To obtain now the wanted spectrum in nadir viewing geometry only a small

200

205

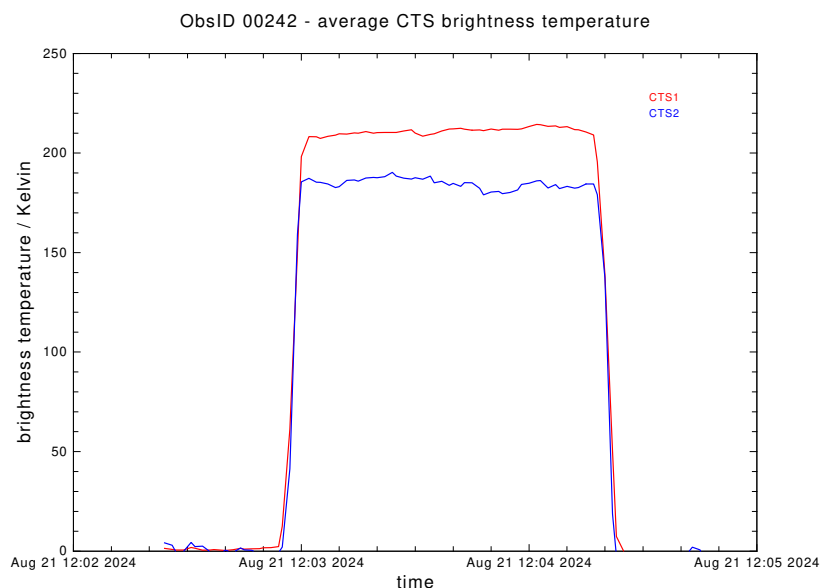


Figure 5. The average brightness temperature (average over the spectrometer channels) versus time for the observation shown in Figure 4. Shown in red are the data obtained with the CTS1 connected to 600 GHz receiver, shown in blue are the data obtained with the CTS2 connected to 1200 GHz receiver. The whole scan across the Earth’s disk took about 90 seconds.

subset of the on-disk pixels around the central pixel have been averaged. During LEGA SWI has executed in total twelve such 1-dimension scans (either in vertical or horizontal direction), which could be used in this way for the intended analysis.

4.1.2 2-Dimensional Maps

210 2-dimensional maps are just an extension of 1-dimensional maps. They are executed as a sequence of 1-dimensional scans where each scan is increasingly being shifted perpendicular to the scan direction. An example of such a 2-dimensional map with equal stepsize in x- and y-direction is shown in Figure 6 and 7. To obtain the wanted nadir viewing spectra only the central nine pixels of the apparent disk have been averaged to a single spectrum. This procedure guarantees to exclude limb contribution from the average. In total eight of such maps have been executed during LEGA, resulting in eight more nadir
215 viewing data points.

4.1.3 Spectral Scan Observations in Nadir Viewing Geometry

Spectral scan observations using the observation mode SWI_SPECTRAL_SCAN_CTS_PS_V1 (see Cavalié et al., 2026, this issue) are the third kind of observations with a clean nadir viewing geometry during LEGA. These observations are of special value because they cover a wide range of local oscillator tunings which are not covered by the 1- and 2-dimensional scans
220 across the Earth. Here the observation scheme actually follows the scheme described in section 2.3. Slightly simplified the basic building block of such observation is as follows:

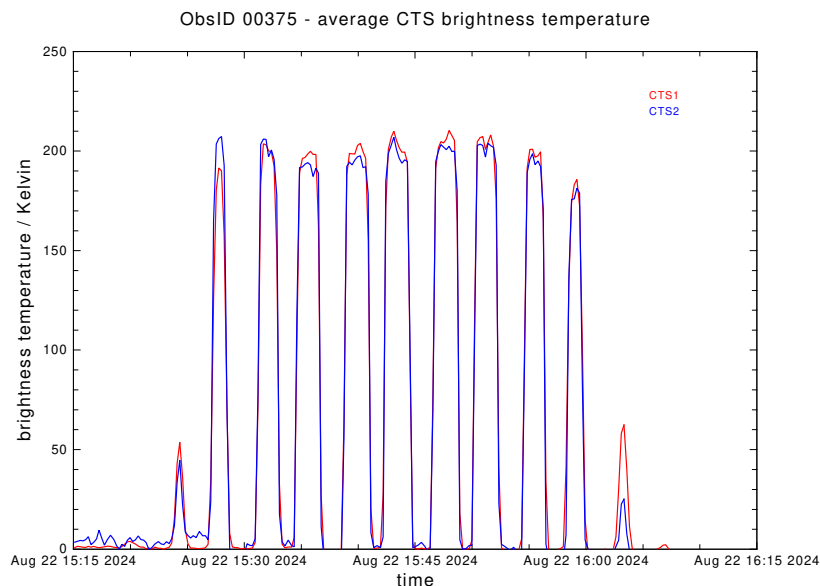


Figure 6. The average brightness temperature versus time for a 2-dimensional 15×15 pixel map of the Earth (ObsID 375). This figure is similar to Figure 5, it can be considered just as a sequence of 1-dimensional scans. Each pixel had an integration time of 14 seconds, the entire map took nearly 1 hour.

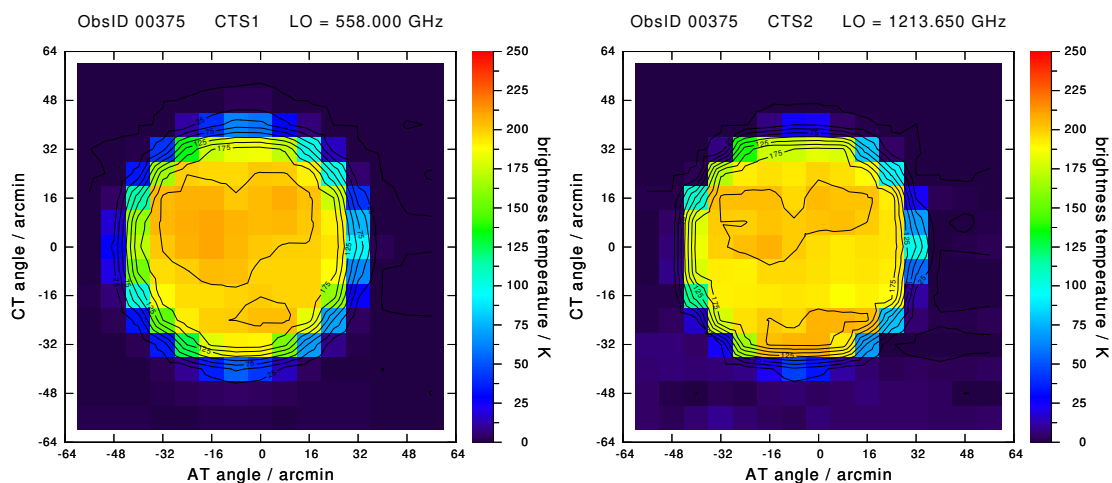


Figure 7. The average brightness temperature data shown in Figure 6 plotted as function of the viewing direction. The data for the 600 GHz receiver are shown on the left, the data for the 1200 GHz receiver are shown on the right. The local oscillator frequency is indicated on top of each panel. The observed sky frequency is actually this local oscillator frequency plus 6 GHz (upper sideband) and minus 6 GHz (lower sideband). The orientation of the Earth is identical to Figure 4, the south pole is at the top of the disk and the equator is slightly below the center of the apparent disk.



1. let SWI view towards the center of the Earth
- 225 2. tune the local oscillator of the 600 GHz and 1200 GHz receiver to the intended frequency
3. take simultaneously spectra with CTS1 and CTS2 (P_a data)
4. let SWI view towards cold sky
- 230 5. take simultaneously spectra with CTS1 and CTS2 (P_c data)

This building block is repeated until the list of intended tunings has been completely processed. In total seven observations with 11 tunings each have been executed during LEGA (see Cavalié et al., 2026, this issue), providing almost 77 further data points for the investigation of the quality of the total power calibration.

4.1.4 Comparison with the Earth Model

235 As previously discussed, in order to save the number of available flip cycles for the Jupiter science phase, nearly all of the data taken during LEGA do not include an observation of the instrument internal hot load. As described in section 2.2, the current idea to still calibrate the data into physical units (i.e. *Rayleigh-Jeans brightness temperature* in Kelvin) is to take the needed noise temperatures T_n from instrument tests performed at other dates. Here we take advantage of the data collected during regular *Payload Checkout Windows* with measurements of system noise temperatures for a fixed set of 75 tunings for each of
240 the two receivers. This receiver health test has been executed during the *Near Earth Commissioning Phase* in June 2023, during the first and second Payload Checkout in January respectively July 2024, and finally a fourth time during Payload Checkout Window 3 in March 2025. So as best estimate for the (not measured) noise temperatures during LEGA the median value for each tuning has been taken. It has been observed empirically that almost all of the noise temperature measurements scatter within just 4% around the corresponding median value. This observation is valid for both the 600 GHz and the 1200 GHz
245 receiver. Because T_n in equation 7 acts as a scaling factor for T_a the immediate conclusion is that the error of the calculated T_a cannot be smaller than 4% of its value. This means a finally calibrated brightness temperature of e.g. 200 K is expected to have an error of $0.04 \times 200 \text{ K} = 8 \text{ K}$. This value defines the task of the comparison with the expected brightness temperature of the Earth Model: do the calibrated data of the LEGA observations fall within a range of $\pm 8 \text{ K}$ around the expected values? This comparison also answers the question of whether the measured system noise temperatures are reasonable at all, or if they are
250 systematically off.

Figure 8 shows the results for the 600 GHz and the 1200 GHz receiver. The red circles show the calibrated brightness temperatures from the observations, the green triangles show the corresponding expected value from the model spectrum of the Earth. Shown as black solid curve is the single sideband model spectrum of the Earth. Because SWI is a double sideband receiver each observation has been plotted versus the corresponding LO-frequency – it must be kept in mind that each symbol represents the
255 signal contribution from a frequency $\pm 6 \text{ GHz}$ apart from the LO frequency. In exactly the same way the expected brightness temperatures (green symbols) have been calculated from the underlying single sideband spectrum. Looking first at the comparison results for the 600 GHz receiver it is obvious that the LEGA data are consistent with the overall shape of the Earth's spectrum. With the exception of only a few outliers we found that 90% of the calibrated brightness temperatures deviate less

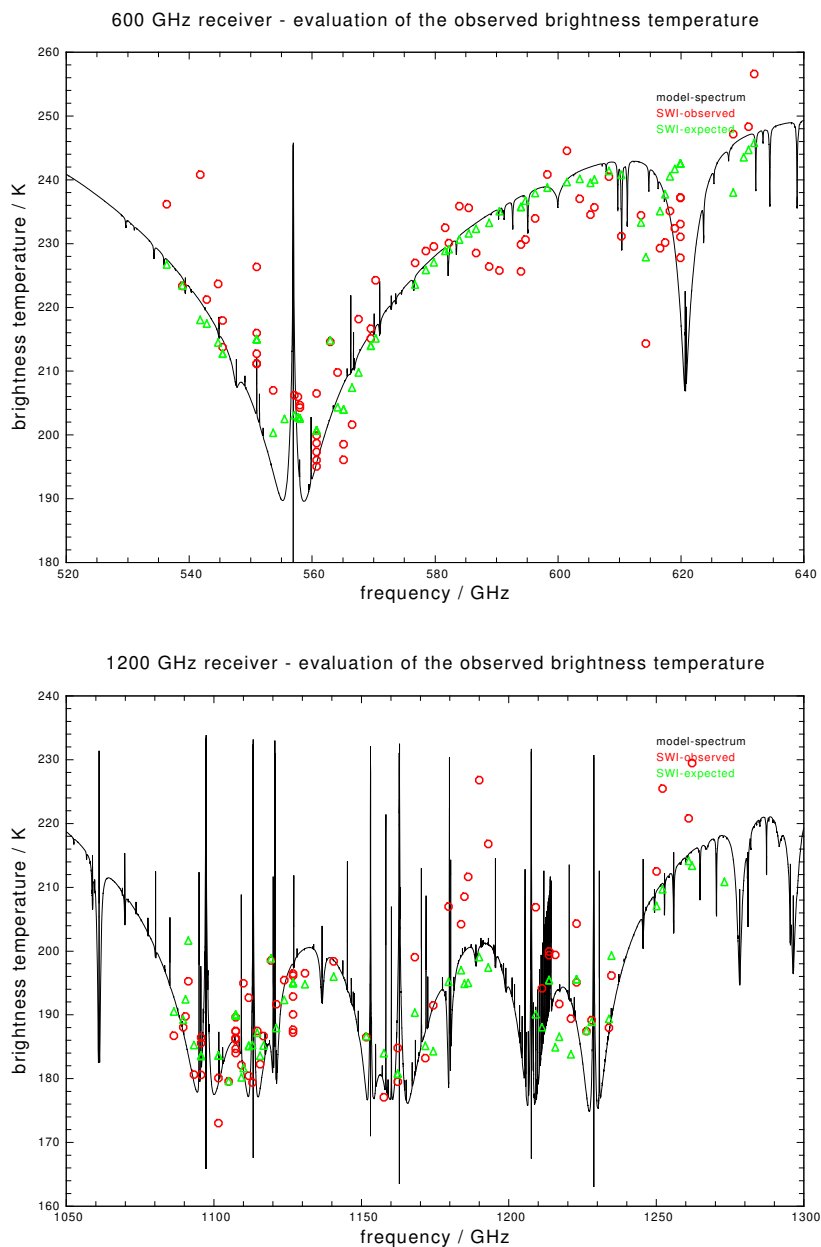


Figure 8. Comparison of the calibrated brightness temperatures (red circles) for the 600 GHz receiver with the expected brightness temperatures (green triangles) from the model of the Earth. Shown as black solid curve is the single sideband model spectrum of the Earth.

than 5% from the expected value, which is close to the value expected from the scatter of the noise temperature measurements.

260 However, the 1200 GHz receiver shows a slightly inconsistent pattern. Up to frequencies of 1170 GHz the deviation of the



measured and expected brightness temperatures is well within the expected 4% deviation, but around 1185 and 1260 GHz the observed brightness temperatures are found to be systematically about 5% to 6% too high. This inconsistent behavior cannot be explained by an inappropriate Earth model, because the data do match the expectations very well within the frequency range of 1080 to 1170 GHz. Instead it is considered to be an instrumental effect and needs more investigation of the SWI hardware behavior itself.

In summary two conclusions can be drawn from this comparison: 1. the noise temperatures measured during commissioning phase and the first three instrument checkouts are valid and accurate – there are outliers, but the data are not consistently off in a systematic way; 2. so far the calibrated data presented in this work do not suggest to introduce any instrument specific or hardware related correction factors, calibration load emissivities, or load coupling efficiencies. The straight forward calibration approach as described in section 2.1 works already well, providing a robust and reliable calibration of the measured output power to the physical quantity of brightness temperature.

4.2 Limb Scan

The small distance of only 6800 km at the Earth's closest approach on 20 August 2024 at 21:57 UTC allowed a very special observation, which can be performed only within a small time window around that event: true limb scanning of the Earth's atmosphere. True limb scanning means that the beam width of the instrument at the tangential point along the viewing direction is much smaller than the thickness of the atmosphere itself. This observation geometry provides the longest path length through the atmosphere and thus the largest amplitude for any spectral line. It is an excellent test case to check within only a minute of observing time if SWI is measuring the correct spectral line shape or if there are any unexpected instrumental effects which severely distort the observed spectra.

The observation scheme was identical to the case of 1-dimensional maps as described in section 4.1.1: spectra have been taken *on-the-fly* without any periodic observations of cold sky in between. The viewing direction of SWI was an inertial pointing chosen to let the Earth drift under SWI's beam during the gravity assist maneuver. The local oscillator of the 600 and 1200 GHz receivers were tuned to 550.980 GHz and 1107.450 GHz, respectively, which allowed to observe in the upper sideband the strong ground state transitions of water vapor at 557 GHz (ortho water) and 1113 GHz (para water). The Earth's limb entered SWI's field of view on 20 August 2024 at 21:20 UTC, 30 minutes before closest approach. At that time the altitude of the Juice spacecraft above ground was 12020 km and the distance to the limb was 17250 km, resulting in a beam width at the limb of 40 km and 23 km for the 600 GHz respectively the 1200 GHz receiver. SWI's beam went across the Earth's disk with a speed of 6.65 km/s, so the limb scan across the 100 km thick atmosphere took only 15 seconds. Because an individual spectrum has been taken every 1.625 seconds the nominal altitude stepsize between individual spectra is 10.8 km – less than the beam width of the instrument for both receivers. In other words the spectra – especially for the 600 GHz receiver – do heavily overlap regarding the sampled altitude range. Figure 9 shows in black the set of observed limb spectra for both the 600 GHz and the 1200 GHz receiver and in red the corresponding set of expected spectra. The 600 GHz receiver spectrum shows the 110–101 target transition of ortho- H_2^{16}O at an IF frequency of 5950 MHz and two additional O_3 transitions at an IF frequency of 5730 resp. 6120 MHz. The 1200 GHz spectrum shows the 111–000 target transition of para H_2^{16}O at an IF frequency of 5900 MHz



295 (upper sideband), the 111–000 transition of para H_2^{18}O at an IF frequency of 5750 MHz (lower sideband), and an O_3 transitions at an IF frequency of 5620 MHz.

The agreement between the expected and observed spectra is excellent, especially the absence of any periodic baseline ripples caused by e.g. standing waves in the instrument optical path demonstrates a high quality of the SWI hardware.

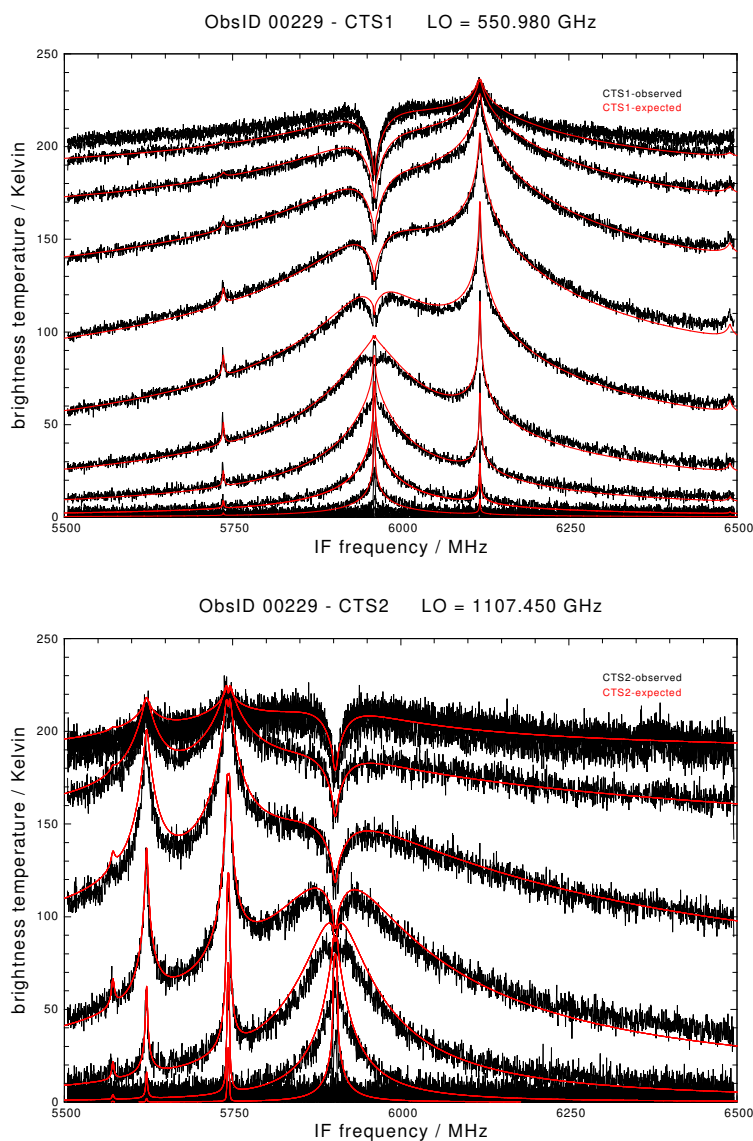


Figure 9. The set of limb spectra (ObsID 229) observed on 20 August 2024 at 21:20 UTC, 30 minutes before closest approach to the Earth. Shown in red are the expected spectra as calculated with the Earth model described in section 3.



4.3 Spectral Scan

300 The scientific purpose of a *Spectral Scan* observation is to explore the spectrum of a science target (Jupiter and the Galilean satellites) over the entire frequency range covered by SWI. This is done by systematically stepping the local oscillator frequency through the entire tuning range of both receivers and to take spectra either in position switching or frequency switching mode. The basic building block of such an observation in position switching mode has been already described in section 4.1.3; for a detailed description of these observing modes see Cavalié et al. (2026, this issue).

305 During the LEGA a large amount of these spectral scan observations have been performed in order to test the implemented observation schemes (also called observation scripts) and also to obtain first information about the behavior and performance of the instrument when the local oscillator frequency is not stable anymore for hours, but changes literally every minute. To evaluate the instrument performance here the Earth signal is once again considered as basically known test signal and deviations from the expected spectra are taken as a strong indicator pointing to unexpected hardware behavior or improper
310 use of the existing hardware. This way it was especially possible to evaluate the entire table of local oscillator settings: which tunings work well, which ones have to be taken with precaution, and which ones do fail and must be marked as unusable.

In the following sections two examples of such spectral scan observations are shown: the first observation made use of the CTS as spectrometer while the second observation used the ACS instead.

4.3.1 CTS

315 Figure 10 shows an example (ObsID 289 and 290) of a position switched spectral scan using the CTS as spectrometer. The pointing direction has been chosen towards the Earth's limb to increase the spectral line amplitude. The black curve shows the observed spectra and the red curve the expected spectra. Contrary to the data shown before in this paper here the y-axis does not provide the brightness temperature in units of Kelvin but instead provides the radiation intensity as a dimensionless number. The reason for this is as follows: most of the tunings executed during the LEGA spectral scan observations have
320 been used for the very first time, but because of the calibration flip mirror issue described in section 2.2, it has been decided not to take spectra of the internal hot load. Consequently we do not have T_n data for all of the tunings. Hence the data can be only partly processed to the quantity $(P_a - P_c)/P_c$. To enable easy comparison with the expected spectra then both – the observed and the expected spectrum – have been *normalized* to unity, i.e. the entire spectrum has been divided by its average: $y_{j,normalized} = y_j / \sum_{j=1}^m y_j$. This way to compare the observed data with the expected spectra has been also applied to the
325 ACS data shown in Figure 11. Here it is not the intention to identify and explain each single detected transition, but instead to show the quality of the observed spectra for a set of well working tunings.

When looking carefully at the spectra a set of weak narrow peaks at IF frequencies of 5600, 5700, 5800, ... MHz are visible. These peaks are actually an instrumental effect, because a frequency comb with 100 MHz fundamental frequency is used for the frequency calibration of the CTS spectra. This calibration signal is turned off before taking science data, but because of a
330 too short delay between the turn off command and the start of the science observation there is still a remainder visible in the science data. Increasing that delay will be the proposed solution to avoid these remainders in future.

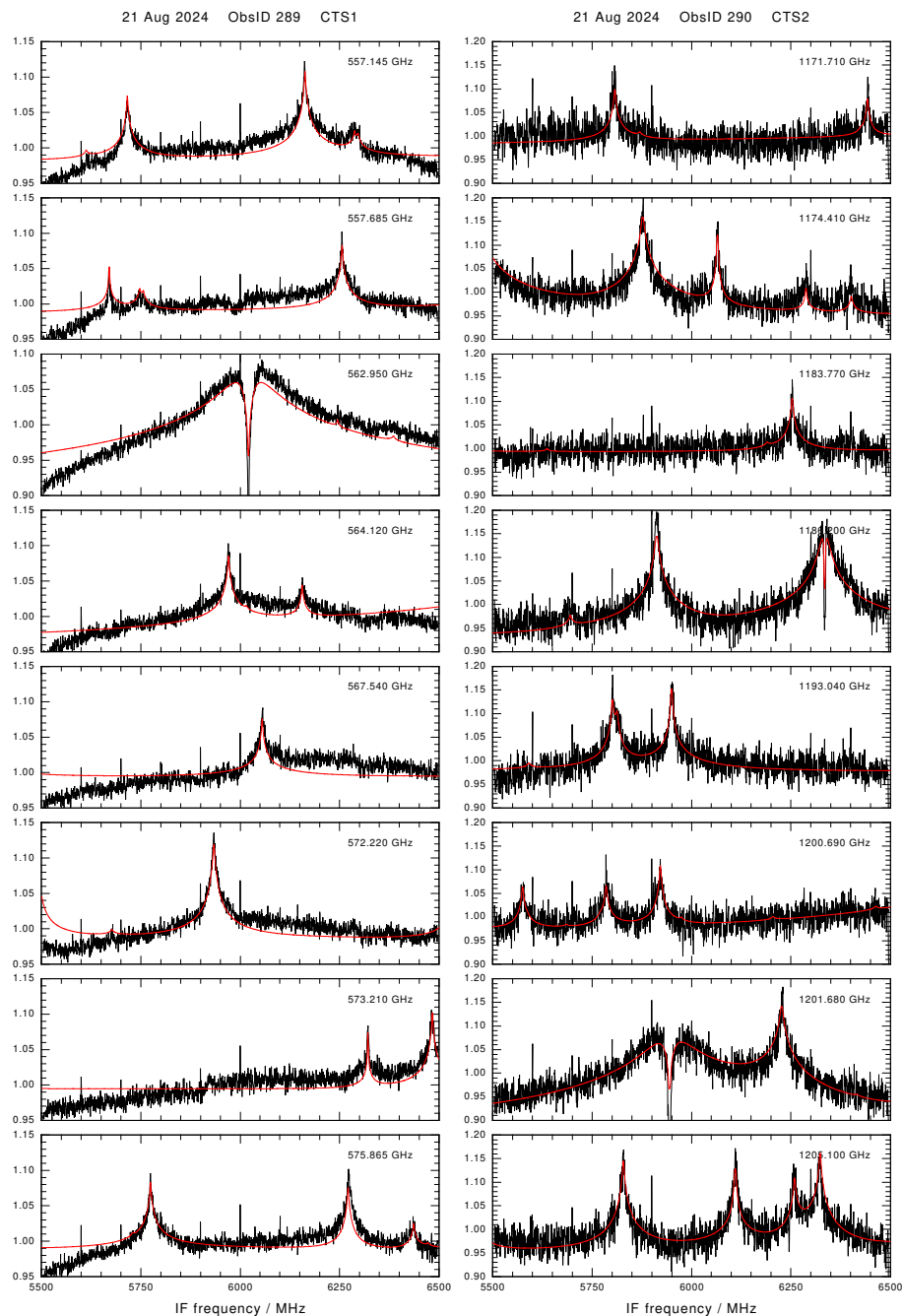


Figure 10. Example of a position switched spectral scan in limb viewing geometry using the CTS as spectrometer. The left column shows spectra obtained with the 600 GHz receiver, the right one those obtained with the 1200 GHz receiver. The local oscillator frequency of each single spectrum is indicated within each panel. The integration time for each individual spectrum was 25 seconds.



4.3.2 ACS

Figure 11 shows an example (ObsID 445 and 450) of a position switched spectral scan using the ACS as spectrometer. In this case the pointing direction has been chosen towards the Earth's nadir direction. This spectral scan demonstrates clearly, how advantageous it is to calculate the expected spectrum as double sideband spectrum, if the observed spectrum is a double sideband spectrum as well. The upper right panel for ACS2 with local oscillator frequency 1212.750 GHz shows at an IF frequency of 5080 MHz the strong 422–413 transition of para-H₂O in the lower sideband of the 1200 GHz receiver. Increasing stepwise the local oscillator lets this transition move to higher IF frequencies and finally leave the IF range analyzed by the ACS. Instead – when further increasing the LO frequency to 1218.870 GHz – a set of ozone transitions are observed in the lower sideband. Continuing to increase the LO frequency lets this ozone pattern move towards higher IF frequencies, but at the same time another strong transition enters the spectrometer's frequency range and is moving in the opposite direction from higher to lower IF frequencies. This transition is the strong 220–211 transition of para-H₂O, but now detected in the upper sideband of the receiver. This spectral transition is actually at a 14 GHz higher sky frequency than the set of ozone transitions, but overlaps with these ozone transitions in the IF. It is clearly visible that this effect is only properly modeled when modeling the expected spectrum also as a double sideband spectrum.

Now looking at all of the spectra for the ACS1 it is obvious that the spectrum for the local oscillator frequency of 563.535 GHz is different from all of the others: it does not match the expected spectrum as well as the other spectra do, though the change in LO frequency is only small. Exactly this is the way how we evaluate the instrument performing for each tuning: if the deviation from the expectation is significantly larger than on average, then that tuning must be flagged 'bad' and not used anylonger until a workaround is found. Without the Earth providing a known and strong test signal this efficient procedure would not have been possible.

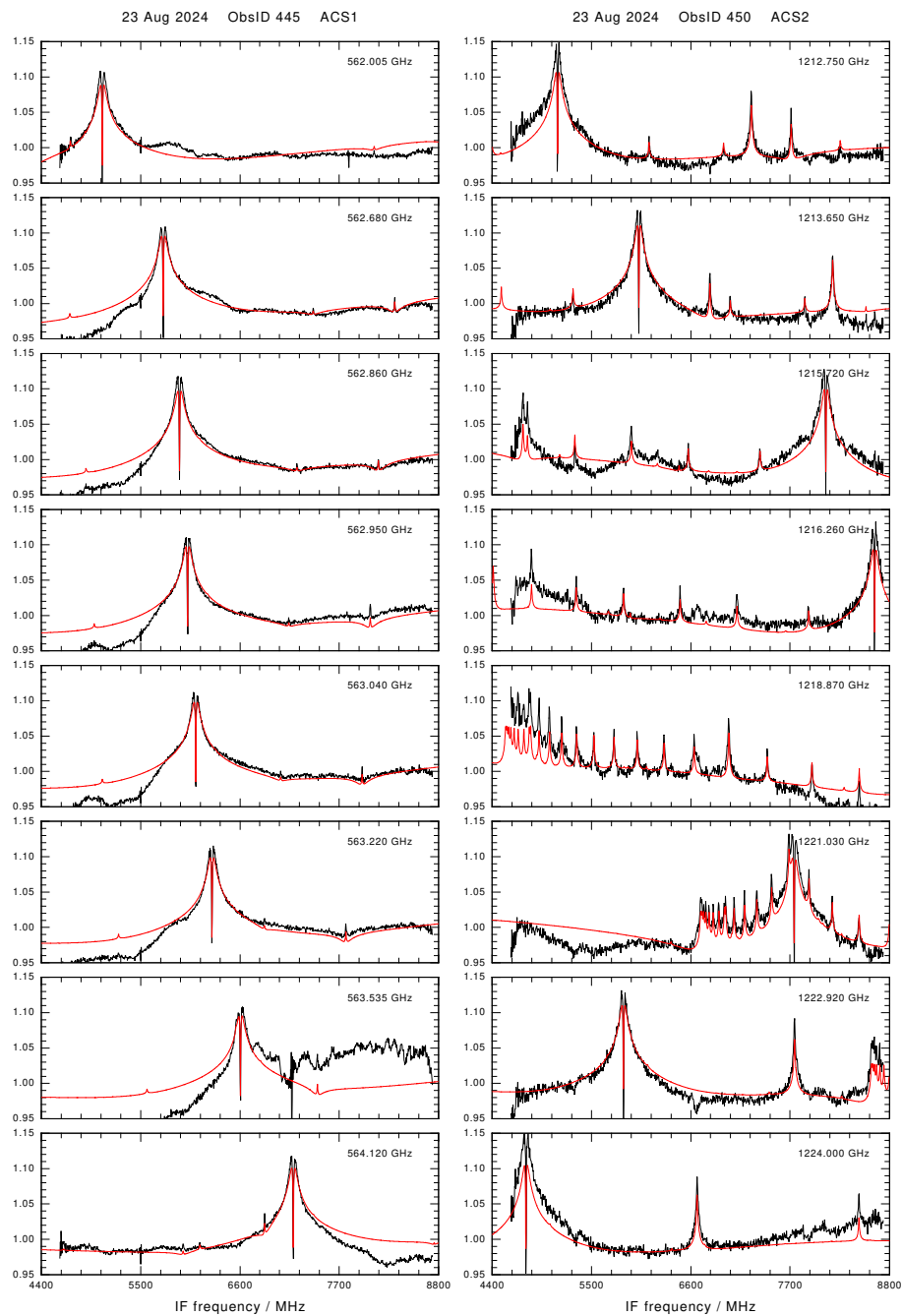


Figure 11. Example of a position switched spectral scan in nadir viewing geometry using the ACS as spectrometer. The integration time for each individual spectrum was 10 seconds.



5 Conclusions

In this paper we present first results of the Earth observations executed with the SWI instrument during the LEGA, which provided a unique opportunity to thoroughly investigate the instrument's performance using the Earth as a known calibration target. The following conclusions have been drawn from the work presented in this paper:

1. The system temperatures as measured in space are valid and can be directly used for the total power calibration of SWI's science data.
2. The system temperatures of both receivers appear to be sufficiently stable to allow a lookup table approach for the total power calibration, which mitigates the limited lifetime problem for the hot load calibration flip mirror.
- 360 3. Obviously the spectra provided by SWI do not show strong and severe standing wave ripples, which are usually present in optical on-axis telescope designs – here SWI clearly benefits from its off-axis telescope design.
4. The instrument internal xy-scanning mechanism (the so-called AT- and CT-mechanism) works reliably: 2-dimensional maps of the Earth are reproducible and do not suffer from severe loss of motor steps.

This work covers just a fraction of the extensive data set of SWI LEGA observations; further work is needed e.g. to complete the total power calibration of the ACS data in order to obtain a comprehensive understanding of the instrument performance.

Code availability. The C-codes used to calculate the expected Earth spectra and to calibrate the observed SWI data is an implementation of published methods. These codes were developed independently by C. Jarchow for internal research purposes, are not publicly released, and may be shared on a case-by-case basis upon justified request.

Data availability. The SWI data acquired during the JUICE Moon–Earth gravity assist in August 2024 are currently under the mission's cruise-phase proprietary period. These data will be made available through the ESA Planetary Science Archive following the first Cruise Archive Delivery, which is currently scheduled for six months after the third Earth Gravity Assist in 2029.

Author contributions. C. Jarchow prepared the original manuscript. L. Rezac contributed to the data analysis and total power calibration. T. Cavalíé, F. Herpin, and R. Moreno defined the LEGA observations which then have been implemented by P. Hartogh and A. Ravanbakhsh. A. Murk provided the MERRA-2 data for the Earth atmosphere model. All co-authors contributed to the successful implementation of SWI and commented the manuscript.

Competing interests. The authors declare no competing interest.



Acknowledgements. Juice is a mission under ESA leadership with contributions from its Member States, NASA, JAXA and the Israel Space Agency. It is the first Large-class mission in ESA's Cosmic Vision programme. SWI has been designed and developed by an international consortium of institutes led by the Max Planck Institute for Solar System Research (MPS, Germany) and including the Laboratory for Studies of Radiation and Matter in Astrophysics (LERMA, France), the Space Research Centre of the Polish Academy of Sciences (CBK, Poland), Chalmers University of Technology (Sweden), the Institute of Applied Physics of the University of Bern (IAP, Switzerland), the National Institute of Information and Communications Technology (NICT, Japan) and the French Space Agency CNES with additional support from the Laboratoire d'Instrumentation et de Recherche en Astrophysique of the Observatoire de Paris (LIRA, France), the Laboratoire d'Astrophysique de Bordeaux (LAB, France), the RPG Radiometer Physics GmbH (Germany), and Omnisys Instrument AV (Sweden). This development has been supported by national funding agencies and other organizations, including the Deutsches Zentrum für Luft- und Raumfahrt (DLR) and by central resources of the Max-Planck-Society. T. Cavalié, F. Herpin and R. Moreno acknowledges funding from the Centre National d'Études Spatiales (CNES). MERRA-2 data are provided by NASA at the Modeling and Assimilation Data and Information Services Center (MDISC).



References

- 390 Cavalié, T., Moreno, R., Rezac, L., Herpin, F., Jarchow, C., Hartogh, P., Carrasco Gallardo, A., Goodyear, S., Mancini, P., Schulz-Ravanbakhsh, A., Dabrowski, B., Kasai, Y., Lellouch, E., Murk, A., Murtagh, D., Olberg, M., Rengel, M., Sagawa, H., Szutowicz, S., and Wirström, E.: JUICE/SWI during the Lunar-Earth-Gravity-Assist. II. Instrument operations, *Annales Geophysicae*, this issue, 2026.
- Gelaro, R., McCarty, W., Suárez, M. J., Todling, R., Molod, A., Takacs, L., Randles, C. A., Darmenov, A., Bosilovich, M. G., Reichle, R., Wargan, K., Coy, L., Cullather, R., Draper, C., Akella, S., Buchard, V., Conaty, A., da Silva, A. M., Gu, W., Kim, G.-K., Koster, R.,
- 395 Lucchesi, R., Merkova, D., Nielsen, J. E., Partyka, G., Pawson, S., Putman, W., Rienecker, M., Schubert, S. D., Sienkiewicz, M., and Zhao, B.: The Modern-Era Retrospective Analysis for Research and Applications, Version 2 (MERRA-2), *Journal of Climate*, 30, 5419–5454, <https://doi.org/10.1175/JCLI-D-16-0758.1>, 2017.
- Global Modeling And Assimilation Office and Pawson, S.: MERRA-2 inst3_3d_asm_Nv: 3d, 3-Hourly, Instantaneous, Model-Level, Assimilation, Assimilated Meteorological Fields V5.12.4., NASA Goddard Earth Sciences Data and Information Services Center, 2015,
- 400 <https://doi.org/10.5067/WWQSQ8IVFW8>, Accessed at 2025-12-17, 2015.
- Hartogh, P., Lellouch, E., Rezac, L., et al.: Submillimetre Wave Instrument (SWI) on board ESA's Jupiter Icy Moons Explorer (JUICE), *Space Sci. Rev.*, in preparation, 2026a.
- Hartogh, P., Rezac, L., Cavalié, T., Jarchow, C., Moreno, R., Schulz-Ravanbakhsh, A., Rengel, M., Yasuko, K., Lellouch, E., Murk, A., Skup, K., and Wirström, E.: JUICE/SWI during the Lunar-Earth-Gravity-Assist. I. General Overview, *Annales Geophysicae*, this issue, 2026b.
- 405 Jarchow, C. and Hartogh, P.: Retrieval of data from ground-based microwave sensing of the middle atmosphere: comparison of two inversion techniques, in: *Global Process Monitoring and Remote Sensing of the Ocean and Sea Ice*, edited by Deering, D. W. and Gudmandsen, P., vol. 2586 of *Society of Photo-Optical Instrumentation Engineers (SPIE) Conference Series*, pp. 196–205, <https://doi.org/10.1117/12.228623>, 1995.
- Jarchow, C. and Hartogh, P.: Analysis of forward models using the singular value decomposition algorithm, in: *Satellite Remote Sensing of Clouds and the Atmosphere II*, edited by Haigh, J. D., vol. 3220 of *Society of Photo-Optical Instrumentation Engineers (SPIE) Conference Series*, pp. 163–173, <https://doi.org/10.1117/12.301156>, 1997.
- 410 Kutner, M. L. and Ulich, B. L.: Recommendations for calibration of millimeter-wavelength spectral line data., *ApJ*, 250, 341–348, <https://doi.org/10.1086/159380>, 1981.
- Moreno, R., Cavalié, T., Rezac, L., Hartogh, P., and Jarchow, C.: JUICE/SWI during the Lunar-Earth-Gravity-Assist. IV. Antenna Pointing and Beam Characterization, *Annales Geophysicae*, this issue, 2026.
- 415 Ossenkopf, V.: The stability of spectroscopic instruments: a unified Allan variance computation scheme, *A&A*, 479, 915–926, <https://doi.org/10.1051/0004-6361:20079188>, 2008.
- Ossenkopf, V.: Optimization of mapping modes for heterodyne instruments, *A&A*, 495, 677–690, <https://doi.org/10.1051/0004-6361:200809619>, 2009.
- 420 Rothman, L. S., Gordon, I. E., Barbe, A., Benner, D. C., Bernath, P. F., Birk, M., Boudon, V., Brown, L. R., Campargue, A., Champion, J.-P., Chance, K., Coudert, L. H., Dana, V., Devi, V. M., Fally, S., Flaud, J.-M., Gamache, R. R., Goldman, A., Jacquemart, D., Kleiner, I., Lacome, N., Lafferty, W. J., Mandin, J.-Y., Massie, S. T., Mikhailenko, S. N., Miller, C. E., Moazzen-Ahmadi, N., Naumenko, O. V., Nikitin, A. V., Orphal, J., Perevalov, V. I., Perrin, A., Predoi-Cross, A., Rinsland, C. P., Rotger, M., Šimečková, M., Smith, M. A. H., Sung, K., Tashkun, S. A., Tennyson, J., Toth, R. A., Vandaele, A. C., and Vander Auwera, J.: The HITRAN 2008 molecular spectroscopic
- 425 database, *J. Quant. Spec. Radiat. Transf.*, 110, 533–572, <https://doi.org/10.1016/j.jqsrt.2009.02.013>, 2009.

<https://doi.org/10.5194/egusphere-2026-1096>

Preprint. Discussion started: 6 March 2026

© Author(s) 2026. CC BY 4.0 License.



Schieder, R. and Kramer, C.: Optimization of heterodyne observations using Allan variance measurements, *A&A*, 373, 746–756, <https://doi.org/10.1051/0004-6361:20010611>, 2001.